Cell

Structure of the DNA Repair Helicase XPD

Huanting Liu,[1,2] Jana Rudolf,[1,2] Kenneth A. Johnson,[1] Stephen A. McMahon,[1] Muse Oke,[1] Lester Carter,[1] Anne-Marie McRobbie,[1] Sara E. Brown,[1] James H. Naismith,[1,*] and Malcolm F. White[1,*]
[1]Centre for Biomolecular Sciences, University of St. Andrews, North Haugh, St Andrews, Fife KY16 9ST, UK
[2]These authors contributed equally to this work.
*Correspondence: jhn@st-and.ac.uk (J.H.N.), mfw2@st-and.ac.uk (M.F.W.)
DOI 10.1016/j.cell.2008.04.029

SUMMARY

The XPD helicase (Rad3 in *Saccharomyces cerevisiae*) is a component of transcription factor IIH (TFIIH), which functions in transcription initiation and Nucleotide Excision Repair in eukaryotes, catalyzing DNA duplex opening localized to the transcription start site or site of DNA damage, respectively. XPD has a 5′ to 3′ polarity and the helicase activity is dependent on an iron-sulfur cluster binding domain, a feature that is conserved in related helicases such as FancJ. The *xpd* gene is the target of mutation in patients with xeroderma pigmentosum, trichothiodystrophy, and Cockayne's syndrome, characterized by a wide spectrum of symptoms ranging from cancer susceptibility to neurological and developmental defects. The 2.25 Å crystal structure of XPD from the crenarchaeon *Sulfolobus tokodaii*, presented here together with detailed biochemical analyses, allows a molecular understanding of the structural basis for helicase activity and explains the phenotypes of *xpd* mutations in humans.

INTRODUCTION

XPD (Rad3 in *S. cerevisiae*) is a superfamily 2 DNA helicase with a 5′-3′ polarity. In eukaryotes, XPD is a component of the transcription factor IIH (TFIIH), along with the helicase XPB (Rad25) and eight other protein subunits. TFIIH is essential for RNA polymerase (RNAP) II-mediated transcription initiation and for the Nucleotide Excision Repair (NER) pathway. In both situations, the role of TFIIH is to open up the DNA duplex, around the promoter or site of DNA damage, allowing access for RNAP or NER factors in the respective pathways. XPD is the structural bridge linking the core TFIIH subunits required for NER to the Cdk-activating kinase (CAK) complex (reviewed in Chen and Suter, 2003). The helicase activity of XPD is not required for transcription initiation, as point mutations that knock out this function while preserving the protein structure result in transcription-competent TFIIH (Winkler et al., 2000). In contrast, mutations that reduce the helicase activity of XPD cause defects in the NER pathway. Mutations of human XPD give rise to three related diseases: xeroderma pigmentosum (XP), trichothiodystrophy (TTD), and combined XP with Cockayne's syndrome (XP/CS) (Lehmann, 2001). These have a surprisingly wide spectrum of symptoms, ranging from severe UV sensitivity and a 1000-fold increased propensity to cancer for XP, through to brittle hair, transcriptional and developmental defects for TTD. This reflects the dual role of TFIIH in transcription and repair. Mouse models for XP/CS and TTD syndromes have highlighted the importance of segmental progeria, or premature aging, that is thought to be a consequence of accumulating DNA damage leading to transcriptional defects and apoptosis (Andressoo et al., 2006; de Boer et al., 2002).

Most archaea encode clear homologs of both the XPD and XPB helicases (Kelman and White, 2005), but no other subunits of TFIIH. We have shown previously that archaeal XPD functions independently as a 5′-3′ DNA helicase, and that the helicase activity is dependent on a small iron-sulfur (FeS) binding domain near the N terminus (Rudolf et al., 2006). This cluster is liganded by four cysteine residues, three of which are absolutely conserved in all archaeal and eukaryotic XPD proteins. Mutation of any of the three conserved cysteines results in disruption of the FeS cluster and a loss of helicase activity, while the fourth is not essential (Rudolf et al., 2006). The importance of the FeS cluster was also demonstrated in *S. cerevisiae*, where disruption of the cluster gave rise to a strong UV-sensitive phenotype in vivo. The human XPD mutation R112H, which inactivates the helicase activity and gives rise to TTD, probably exerts its effect by disrupting the FeS cluster (Rudolf et al., 2006).

XPD is the founding member of a family of DNA helicases in eukaryotes, which includes the FancJ (also known as Bach1, Brip1), Chl1, and Tel helicases. These helicases are involved in a variety of DNA repair and recombination pathways in humans, and all have the conserved cysteine residues diagnostic for the FeS cluster. Some mutations of FancJ that cause Fanconi anemia map close to the FeS domain, suggesting that the FeS cluster is also essential for this enzyme (Pugh et al., 2008; Rudolf et al., 2006).

The role of the FeS cluster in XPD and related helicases has not been defined. The observation that the FeS domain is conserved in a family of helicases with different functions suggests that it is not specialized for the detection of DNA damage, but rather that it plays a generic role for these helicases. Although FeS cluster-containing proteins are often involved in redox reactions, examples of FeS clusters in a variety of proteins including DNA

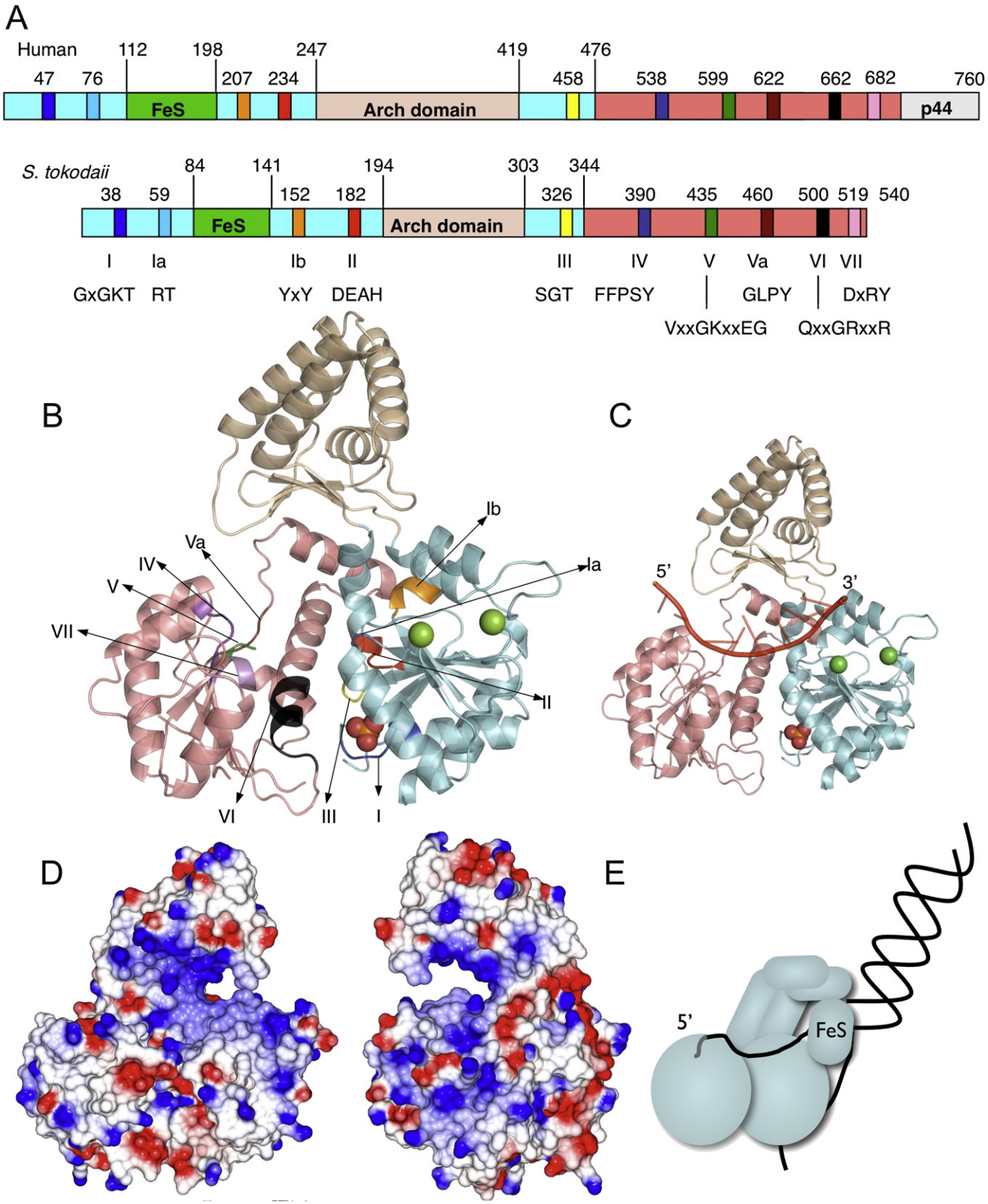
A
Human
112
198
247
419
476
47
76
207
234
458
538
599
622
662
682
760
FeS
Arch domain
p44
S. tokodaii
84
141
194
303
344
38
59
152
182
326
390
435
460
500
519
540
FeS
Arch domain
I
Ia
Ib
II
III
IV
V
Va
VI
VII
GxGKT
RT
YxY
DEAH
SGT
FFPSY
VxxGKxxEG
GLPY
QxxGRxxR
DxRY
B
Ib
Va
IV
V
Ia
VII
II
VI
III
I
C
5'
3'
D
E
5'
FeS

primase (Klinge et al., 2007), RNA polymerase (Hirata et al., 2008) and DNA glycosylases (Hinks et al., 2002; Kuo et al., 1992) suggest that FeS clusters can have a purely structural role, analogous to other metal binding domains. SF1 and SF2 helicases have two conserved motor domains with a RecA fold, which couple ATP hydrolysis to translocation along DNA or RNA strands (reviewed in Singleton and Wigley, 2002). In addition, they frequently have accessory domains specific for nucleic acid or protein interactions. XPD mutants with a disrupted FeS domain still bind to ssDNA and have DNA-dependent ATPase activity, suggesting that the function of the domain may be to physically separate the strands of the DNA duplex (Pugh et al., 2008; Rudolf et al., 2006). There are several examples of accessory domains organized as inserts to the helicase motor domains that are required for the physical separation of duplex DNA—for example the beta-hairpin domains of the bacterial DNA repair helicase UvrB (Theis et al., 1999) and the archaeal SF2 helicase Hel308 (Buttner et al., 2007).

We now present the X-ray structure of XPD from the archaeon *Sulfolobus tokodaii*, to the best of our knowledge, the first reported structure of an SF2 5′ to 3′ helicase. The XPD structure allows a molecular interpretation of a number of naturally occurring human mutations that lead to severe human diseases.

RESULTS

Overview of the Structure of XPD

Archaeal and eukaryal XPD proteins share 25% sequence identity, which includes the seven conserved canonical motifs identified in the SF2 helicase family (motifs I, Ia, II–VI) (Gorbalenya and Koonin, 1993) (Figure 1A, Figure S1 available online). The structure of XPD from the crenarchaeon *S. tokodaii* was solved at 2.25 Å resolution, and crystallographic statistics are given in Table 1. There are three major domains (Figure 1B). The two canonical motor domains (1 and 2) that are present in all SF1 and SF2 helicases are a good structural match for those in other helicases, matching with a 2.8 Å rmsd over 201 common Cα positions in the NS3 helicase, for example (Figure S2). The two motor domains have a central interface in which ATP is bound and hydrolyzed. In our apo-structure, a phosphate ion is bound at the predicted catalytic site. The motion of the two motor domains relative to one other during ATP binding and hydrolysis drives DNA translocation. The canonical motifs I, II, III, V, and VI are known from other helicases to be involved in ATP binding (reviewed in Singleton et al., 2007) and are present in equivalent positions in XPD, although motif V is unstructured in our apo-structure (Figure 1B). Motifs Ia, IV, and V are known to interact with the nucleic acid substrate in other helicases, and map to the upper surface of motor domains 1 and 2 (Figure 1B). Additionally, we identify conserved sequence motifs Ib (YxY), Va (GLPY), and VII (DxRY) in XPD family members that are positioned to interact with the ssDNA substrate.

A third domain, which we term the Arch domain (residues 194–303), has a mixed α β topology with a four-stranded antiparallel

Table 1. Crystallographic Statistics for Data Collected from Crystals of Native and Selenomethionine-Labeled XPD

Data Collection	Refined Structure	SeMet Peak	SeMet Remote
λ (Å)	1.06	0.9787 anom. pairs unmerged	0.9749 anom. pairs unmerged
Resolution (Å)	28 – 2.25	30 – 2.7	30 – 2.7
Last shell (Å)	2.32–2.25	2.8–2.7	2.8–2.7
Spacegroup	$P2_12_12$	$P2_12_12$	
Cell (Å)	A = 95.7, b = 100.3, c = 62.5	a = 94.5, b = 98.6, c = 63.1	
Unique refl's	29129(2891)	31109(3103)	31244(3214)
Average redundancy	6.2(3.9)	4.3(4.2)	8.6(8.5)
I/σ	26.3(3.0)	23.0(2.8)	26.1(2.7)
Complete (%)	99.4(97.4)	99.5(96.5)	99.9(100.0)
R_{merge} (%)	5.6(42.9)	4.5(52.0)	6.0(84.5)
Seleniums found		11 of 13	
Refinement			
R %	23.2 (28.7)		
R_{free} %	27.6 (32.9)		
rmsd bonds (Å)/ angles (°)	0.010/1.197		
Ramach'n favored (%)	96		
PDB accession code	2VL7		

The numbers in parentheses refer to the last shell.

Figure 1. Structure of XPD

(A) Comparison of the domain organization of human and *S. tokodaii* XPD. Motor domain 1 is shown in cyan, motor domain 2 in salmon, the Arch domain in wheat and the FeS domain in green. The positions of the canonical motifs are shown by colored bars, and the conserved sequences of these motifs are indicated. The C-terminal region of human XPD that interacts with the p44 protein is shown as a gray box, and is not present in the archaeal XPD.

(B) Overview of the structure of XPD. Domains are colored as in 1A. The Arch domain (top of structure) arises as an insert into motor domain 1. The boundaries of the FeS cluster binding domain, which is not visible in the electron density map, are indicated by green spheres. The canonical motifs defined in (A) are indicated with the same color scheme and labeled. The phosphate ion in the ATP binding site is shown space-filled.

(C) *S. tokodaii* XPD is shown in the same orientation and color scheme as in (B). The DNA species shown as a red cartoon is taken from the cocrystal structure of the 3′ to 5′ helicase Hel308 (PDB code 2p6r). The position of the DNA arises as a consequence from an overlay of the motor domains of the two enzymes without any further modeling.

(D) GRASP representation of the electrostatic surface of XPD shown in the same orientation as (B) (left) and with a rotation of 90° (right). The narrow channel formed between the Arch domain and motor domain 1 is lined with basic residues, and could accommodate ssDNA but not duplex DNA.

(E) Cartoon showing the likely path of DNA through the XPD helicase. Duplex DNA entering from the right is broken on the FeS domain, threading through the cleft between the Arch domain and motor domain 1, engaging with the conserved helicase motifs Ia, Ib, IV, V, Va, and VII. The orphaned (3′) strand of the duplex may form interactions with the basic surface on the outside of the motor domain, shown in the right panel of 1D.

β sheet and four α-helices. There is no convincing match in the protein databank (PDB) for the fold of the Arch domain, suggesting this region represents a novel fold. The Arch domain is an insertion into a loop of motor domain 1, sitting above the central cleft between the two motor domains and making contact with both. The Arch domain sequence is not highly conserved in XPD family members, and is 60% larger in the eukaryotic XPDs. This may provide further interaction surfaces with components of TFIIH, including the CAK complex, which anchors to the TFIIH core via an interaction with XPD (Chen et al., 2003).

The FeS domain (residues 84–141) is also an insertion in motor domain 1. This small domain is disordered in our structure and its boundaries are shown by green spheres in Figure 1B. The FeS domain occupies a position above motor domain 1, equivalent to the β-hairpin loop in the helicase UvrB (Theis et al., 1999) (Figure S2B). UvrB is not, overall, a close structural match for XPD (Rudolf et al., 2006), but carries out the analogous NER step in bacteria. This predicted position would match the loops seen in other helicases that have been termed the ''plowshare,'' and which function to separate the two strands of the DNA duplex as single-stranded DNA is drawn across the top of the motor domains.

The XPD structure is the first of an SF2 helicase with a 5′ to 3′ polarity, and helps explain the factors important for the determination of translocation polarity in helicases. As for the NS3 helicase, the motor domains of the 3′ to 5′ SF2 helicase Hel308 can be overlaid with those of XPD. This modeling positions the ssDNA strand of the DNA substrate co-crystallized with Hel308 (Buttner et al., 2007) across the top of the XPD motor domains (Figure 1C). The duplex portion of the Hel308 DNA substrate (not shown) is on the left of XPD motor domain 2. Given that XPD has the opposite polarity to Hel308, the duplex DNA is predicted to be unwound on the opposite side of XPD, at domain 1. This is consistent with the proposed role for the FeS cluster domain in the physical separation of the DNA duplex strands (Pugh et al., 2008; Rudolf et al., 2006). ssDNA would then pass across the tops of domains 1 and 2 with the same polarity as the DNA strand labeled in Figure 1C. The Arch domain bends over the top of domain 1, forming a channel that could accommodate single-stranded but not duplex DNA. The electrostatic surface of the XPD protein shows a highly basic surface lining the narrow channel formed between the Arch domain and domain 1 (Figure 1D). In addition, there is a basic surface on the back of domain 1 that may interact with the orphaned 3′ ssDNA strand. By analogy with other DNA helicase structures, we propose that the Arch domain and Fe-S loop collaborate to break the DNA duplex and channel the 5′ ssDNA end across the top of the two motor domains, where it makes contact with the DNA binding motifs on the motor domains (Figure 1E). This is supported by recent biochemical experiments that place the FeS domain near the junction of ssDNA and dsDNA (Pugh et al., 2008).

XP-Causing Mutations

XP-causing mutations tend to cluster in the helicase motifs, and the residues whose mutation in human XPD gives rise to xeroderma pigmentosum are all conserved in archaeal XPD (Figure 2A, Figure S1). These observations support the theory that XP is caused by mutations that inactivate the helicase without disrupting the structure, by targeting conserved catalytic or DNA and ATP binding residues. These mutations are mapped onto the XPD structure in Figures 2B and 2C. The likely path of ssDNA is shown using the 8 deoxyuridine (8 dU) strand from the crystal structure of the NS3 helicase (Kim et al., 1998). This nucleic acid sequence has been placed without modeling, based solely on the structural overlay between the motor domains of XPD and NS3 (Figure S2A). Five of the residues targeted by XP-causing mutations: (*S. tokadaii* residues with human mutations in parenthesis) R365 (R511Q), S393 (S541R), Y394 (Y542C), D519 (D681N), and R521 (R683Q/W) cluster on the top surface of domain 2 adjacent to the predicted route of the ssDNA (Figures 2B and 2C). R683 is mutated in 75% of all known XP-D mutations (Taylor et al., 1997). A sixth residue, T60 (T76A), is in a suitable position to engage with the ssDNA at the top of domain 1. Of the remaining residues, D182 (D234N, not shown for clarity) targets the Walker B motif involved in ATP hydrolysis while R437 (R601L/W) is not visible in the structure but is part of motif V and predicted to lie close to the cluster of residues interacting with ssDNA in domain 2.

XP/CS-Causing Mutations

The combination of XP and CS phenotypes is associated with rare mutations in XPD, XPB and XPG (Dupuy and Lafforet, 1978). Patients suffer a combination of a classical XP phenotype along with the severe neurological and developmental abnormalities of CS (Lehmann, 2003). Four XPD mutations that give rise to XP/CS are known: G47R, G602D, R666W, and G675R (Theron et al., 2005) (Figure 2A). In structural terms, the observation that three of the known XP/CS mutations target glycine residues is provocative, given the unique role of glycine in providing conformational flexibility in a polypeptide chain. Studies of cells from a XP/CS patient (van Hoffen et al., 1999) revealed decreased TFIIH levels and an inability to remove UV damage from DNA coupled with an increased level of incision of undamaged DNA. This was recently confirmed in a mouse model of XP/CS harbouring the XPD G602D mutation (Andressoo et al., 2006). The combined XP and CS phenotypes suggest that these mutations must have some effect on TFIIH structure and stability, giving rise to transcriptional defects that are distinct from those generated by TTD mutations. In the structure, A438 (G602D) lies next to the XP-targeted residue R437 (R601L/W) on a mobile region of motif V, which is implicated in both ATP and ssDNA binding. G38 (G47R) and R507 (R666W) are positioned close to the ATP binding site in the interface between motor domains 1 and 2. Mutations in this region may interfere with the coupling of ATP hydrolysis to DNA translocation. V513 (G675R) sits near the bottom of domain 2, well away from the ssDNA and ATP binding sites and close to a cluster of residues known to be involved in the interaction with the p44 protein.

TTD-Causing Mutations

In marked contrast to the situation for XP mutations, only two out of twelve residues mutated in TTD are conserved in archaeal XPD (Figures 3A and S1). We showed previously that R112, which is conserved as a lysine or arginine in archaeal XPDs, is important for the stability of the FeS cluster binding domain, suggesting that this mutation may destabilize XPD to some extent

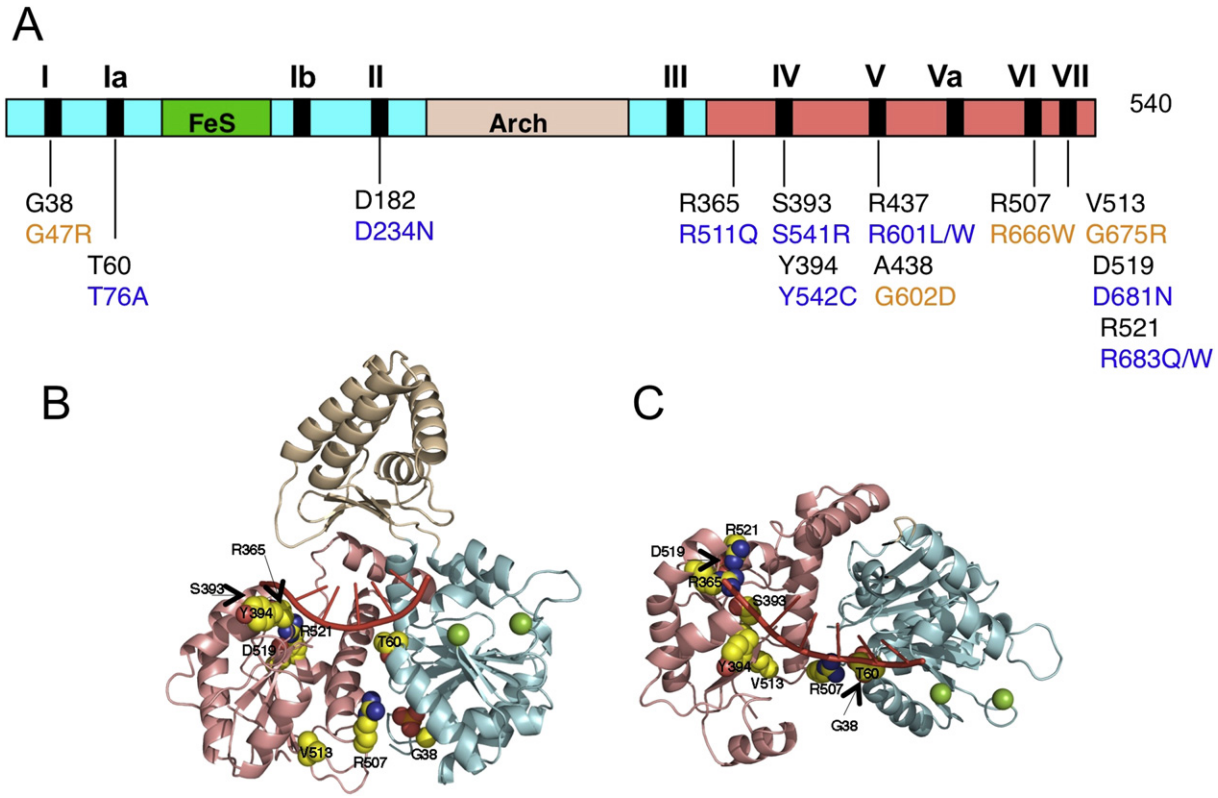

Figure 2. Mutations of XPD Giving Rise to XP and XP/CS

(A) Schematic showing the domain structure and canonical motifs of *S. tokodaii* XPD. Domain boundaries are colored as in Figure 1A, and canonical motifs indicated with black bars. The positions of residues targeted by mutation in XP and XP/CS are indicated, with the *S. tokodaii* residue and numbering in black and the equivalent human residue numbering indicated immediately below in blue (XP) or orange (XP/CS).

(B) Structure of *S. tokodaii* XPD, colored as in Figure 1B, with the 8-mer dU oligonucleotide derived from the co-crystal structure of the NS3 helicase shown in red (see also Figure S2). Residues mutated in XP and present in the *S. tokodaii* crystal structure are shown as space-filled sphere models, colored by element (carbon, yellow; nitrogen, blue; oxygen, red). Residues R437 and A438 constitute part of the loop formed by motif V that is not observed in the crystal structure. Residue D182, in motif II (the Walker B box) is omitted for clarity.

(C) Details as for (B), with the structure rotated vertically forward by 90°. The Arch domain is omitted for clarity. The cluster of residues at the top of domain 2 close to the expected position of the ssDNA is apparent.

(Rudolf et al., 2006). G428 (R592P) and Y430 (A594P) sit on the surface of the protein at the bottom of domain 2, well away from the catalytic site of the enzyme (Figure 3C). The mutation G595R in *S. cerevisiae* Rad3 (corresponding to G593R in human XPD) maps to the same area of the protein and reduces the Rad3-mediated inhibition of short sequence recombination (Lee et al., 2000). Similarly, residues E454 (R616P) and D511 (D673G) group in the same area of the XPD protein surface (Figure 3C). This cluster of mutations is in close proximity to the eukaryotic XPD p44 interaction domain at the C terminus of the protein, and it has been shown that the R616P/W mutants fail to interact with p44 in vitro (Dubaele et al., 2003). These mutations are thus likely to exert their phenotype by destabilizing the interaction with p44 rather than destabilizing XPD directly.

Other TTD-causing mutations are likely to result in the direct destabilization of the XPD structure. For example, I496 (R658H/C) forms part of the interface between the two motor domains while T501 (C663R), points into the core of domain 2. Both these mutations are likely to directly reduce the stability of human XPD (and therefore TFIIH). It is particularly interesting to note that TTD patients carrying the R658C mutation experienced episodes of hair loss during bouts of pneumonia due to elevated body temperature—a classic temperature-sensitive phenotype that indicates decreased XPD and TFIIH stability (Vermeulen et al., 2001). Finally, residue A206 (corresponding to TTD mutation C259Y) points into the center of the helical bundle of the Arch domain (Figure 3D) where it packs closely with other residues constituting the core of this domain. A bulky tyrosine residue at this position in the human enzyme would be predicted to destabilize the Arch domain. Mutation of the equivalent residue in *S. acidocaldarius* XPD, A204Y, resulted in an active enzyme that was temperature sensitive (Figures 3E and 4), consistent with the theory that the C259Y mutation in TTD patients destabilizes the XPD protein structure directly, in turn destabilizing the TFIIH complex.

Biochemical Analyses of XPD Mutations

The structure of XPD has allowed predictions to be made concerning the molecular basis for many of the mutations found in human XPD. To test the predictions, we studied the in vitro

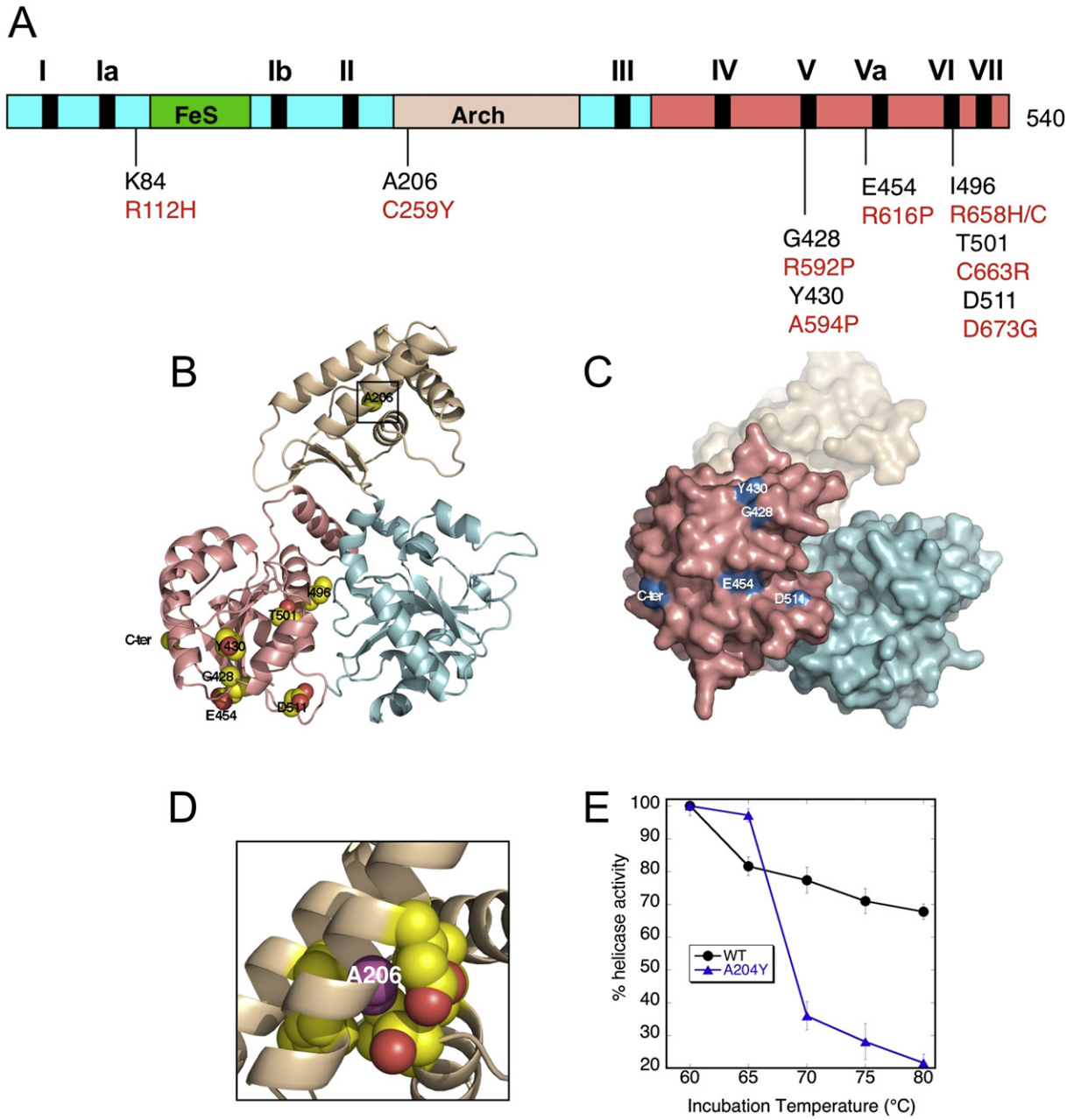

Figure 3. Mutations of XPD Giving Rise to TTD

(A) Schematic showing the domain structure and canonical motifs of *S. tokodaii* XPD. The positions of residues targeted by mutations causing TTD in human are indicated. *S. tokodaii* residues and numbering are in black and the equivalent human residue numbering indicated immediately below in red.

(B) Structure of *S. tokodaii* XPD colored as in Figure 1. The residues targeted by TTD-causing mutations are represented in space-filled and labeled sphere models as in Figure 2B. Residue K84 is on the boundary of the FeS domain and is not visible in the crystal structure. The position of the C terminus in the archaeal XPD protein is also indicated.

(C) XPD structure with surface representation. The model is colored as in 3B and rotated 90° with respect to 3B to emphasize the bottom of domain 2. TTD mutations mapping to the bottom surface of motor domain 2 are colored blue and labeled. In eukaryotic XPD, these residues together with the C-terminal extension probably form an interaction surface with the p44 protein.

(D) Zoomed-in view of the boxed region of the Arch domain in Figure 3B. Residue A206 and surrounding residues are shown as space-filled molecular representations, with A206 in purple and other residues colored according to their atom type. The TTD mutation introducing a tyrosine at this position (C259Y) is likely to cause significant disruption to the core of the Arch domain.

(E) Plot showing the temperature stability of the wild-type and A204Y mutant XPD enzymes from *S. acidocaldarius* (equivalent to *S. tokodaii* A206Y and human C259Y). The helicase activity of the A204Y mutant is similar to that of the wild-type protein, but the mutant enzyme was inactivated on heating for 20 min at the temperatures indicated before assaying for helicase activity. This confirms the predicted destabilizing effect of the C259Y mutation. Data points are means of triplicate experiments and standard errors are shown.

biochemical properties of a selection of mutants generated in the XPD protein from *S. acidocaldarius*. These mutants were expressed and purified in *E. coli* (Figure S3) and tested for ATPase and helicase activities, and in some cases for ssDNA binding affinity. This results in three numbering systems corresponding to *H. sapiens*, *S. tokodaii*, and *S. acidocaldarius*, which can be cross-referenced in Figure 4D; here we will indicate the mutation made in *S. acidocaldarius* with the equivalent human mutation in parenthesis. Three XP-causing mutations, R373Q (R511Q), R531Q and R531W (R683Q/W) were generated and studied. These mutants purified as for the wild-type enzyme and were thermostable, suggesting that they caused no significant structural perturbation. All three mutants were active ssDNA-dependent ATPases, with ATPase activities of approximately 50% of the wild-type level for R373Q and R531W, and 170% for R531Q. All three mutations resulted in weaker ssDNA binding affinity, most pronounced in the R531W mutant, and were not active as helicases. Taken together, these observations are consistent with a role for these residues in helicase activity via interactions with the translocating ssDNA, as suggested from the structural analysis and consistent with the XP phenotype in humans. The elevated ATPase activity seen for R531Q may reflect an uncoupling of ATP hydrolysis and DNA translocation as observed previously for the XPD and PcrA helicases (Rudolf et al., 2006; Soultanas et al., 2000). Two TTD-causing mutations were also mimicked: A204Y which gives rise to an active but less stable enzyme as discussed previously, and D521G (D673G). The latter mutation causes no significant change in the ATPase, helicase or DNA binding parameters compared to the wild-type enzyme, as expected for a mutation that is thought to destabilize the interaction of XPD with p44 (Dubaele et al., 2003).

Two XP/CS mutants, G447D (G602D) and C523R (G675R), were expressed and characterized. Both were thermostable, suggesting no serious destabilization of the protein. Both mutations resulted in a severe decrease in the ssDNA-dependent ATPase activity of XPD, and an abrogation of the helicase activity. The G447D (G602D) mutation targets helicase motif V, which is mobile in the structure and spans the ATP binding and ssDNA binding sites, so a significant decrease in ssDNA stimulated ATP hydrolysis is clearly plausible. The dramatic consequences of the C523R (G675R) mutation are less readily explainable. The G675R mutant in eukaryotic XPD abolishes the interaction with p44 in vitro (Dubaele et al., 2003), consistent with its position near the bottom of domain 2. Unlike the TTD mutations in this area, the G447D mutation in archaeal XPD abolishes the helicase activity, which must be a consequence of a direct effect on catalysis. Thus it seems most likely that this mutation in human XPD has two consequences: a reduced helicase activity, possibly via effects on the ATP-driven conformational cycling that is essential for the helicase activity, and a destabilization of TFIIH.

DISCUSSION

Helicase Polarity and the Role of the FeS Cluster Domain

The XPD structure is the first of a SF2 helicase with a 5′ to 3′ polarity, or SF2B according to the recently suggested nomenclature (Singleton et al., 2007). The overall structure, with two canonical motor domains and two unique accessory domains, conforms well to the paradigm established from structural studies of the NS3, PcrA, UvrD, Hel308 and other helicases. Although DNA is not present in the structure, the positions of the Arch and FeS domains argue strongly that ssDNA is bound in the same orientation as in 3′ to 5′ polarity enzymes and that the enzyme simply translocates in the opposite direction. The same argument has been put forward for RecD, the 5′ to 3′ SF1 helicase subunit of bacterial RecBCD (Singleton et al., 2004). This orientation matches that proposed by Spies and co-workers, based on quenching of fluorescent DNA by the FeS domain in XPD from *Ferroplasma acidarmanus* (Pugh et al., 2008).

The discovery of an essential FeS cluster-binding domain in the XPD helicase prompted speculation as to its role. On the one hand, FeS clusters are typically found in enzymes in a redox-active form where they play a role in electron transport. This raised the possibility that these helicases use the FeS cluster to detect oxidative stress, or even to detect DNA damage directly, as has been proposed for other FeS-containing DNA repair proteins (Boal et al., 2005). XPD is related to three other eukaryotic helicases, FancJ, RTel, and Chl1, all of which have at least three cysteine residues required as FeS cluster ligands. The observation that the FeS domain is found in a variety of helicases with different functions suggests strongly that the role of the cluster is not to detect specific forms of DNA damage, but rather to function as a generic component of the helicase. This supports the theory that the FeS cluster in these helicases is a structural feature that stabilizes a small domain that physically separates the DNA duplex strands.

A structural role for the FeS domain in XPD-family helicases is also supported by bioinformatic analysis of the bacterial DinG helicase, the closest bacterial homolog of XPD (Figure S4). On the one hand, many DinG orthologs are predicted to have an FeS domain in an equivalent position to XPD (Rudolf et al., 2006), and this has been confirmed biochemically for *E. coli* DinG (Voloshin and Camerini-Otero, 2007). However, sequence analysis shows that other DinG sequences, such as that of *Staphylococcus aureus* (Uniprot accession number Q6GGV4), have no cysteine residues in this region of the protein and therefore no possibility of liganding an FeS cluster. We have confirmed this prediction by overexpressing the *S. aureus* DinG protein in *E. coli*—the purified protein is an active helicase and contains no iron (A.-M.M., unpublished data). Consistent with the hypothesis that the FeS cluster has a purely structural role, these organisms appear to have evolved an alternative domain structure that obviates the requirement for the cluster.

Toward a Molecular Understanding of XPD Mutation Phenotypes

The complex spectrum of phenotypes arising from mutation of the *xpd* gene in humans has been the source of much discussion and debate. XP-causing mutations are the simplest to understand, manifesting as NER-defective but transcription-normal in eukaryotic systems. They have been predicted to exert their effect by reducing the helicase activity of XPD without affecting the structure of TFIIH. In contrast TTD mutations have been predicted to disrupt the structure or stability of TFIIH and thus to exert effects on both transcription and NER (Lehmann, 2003). Consistent with these ideas, TTD linked mutants of XPD result

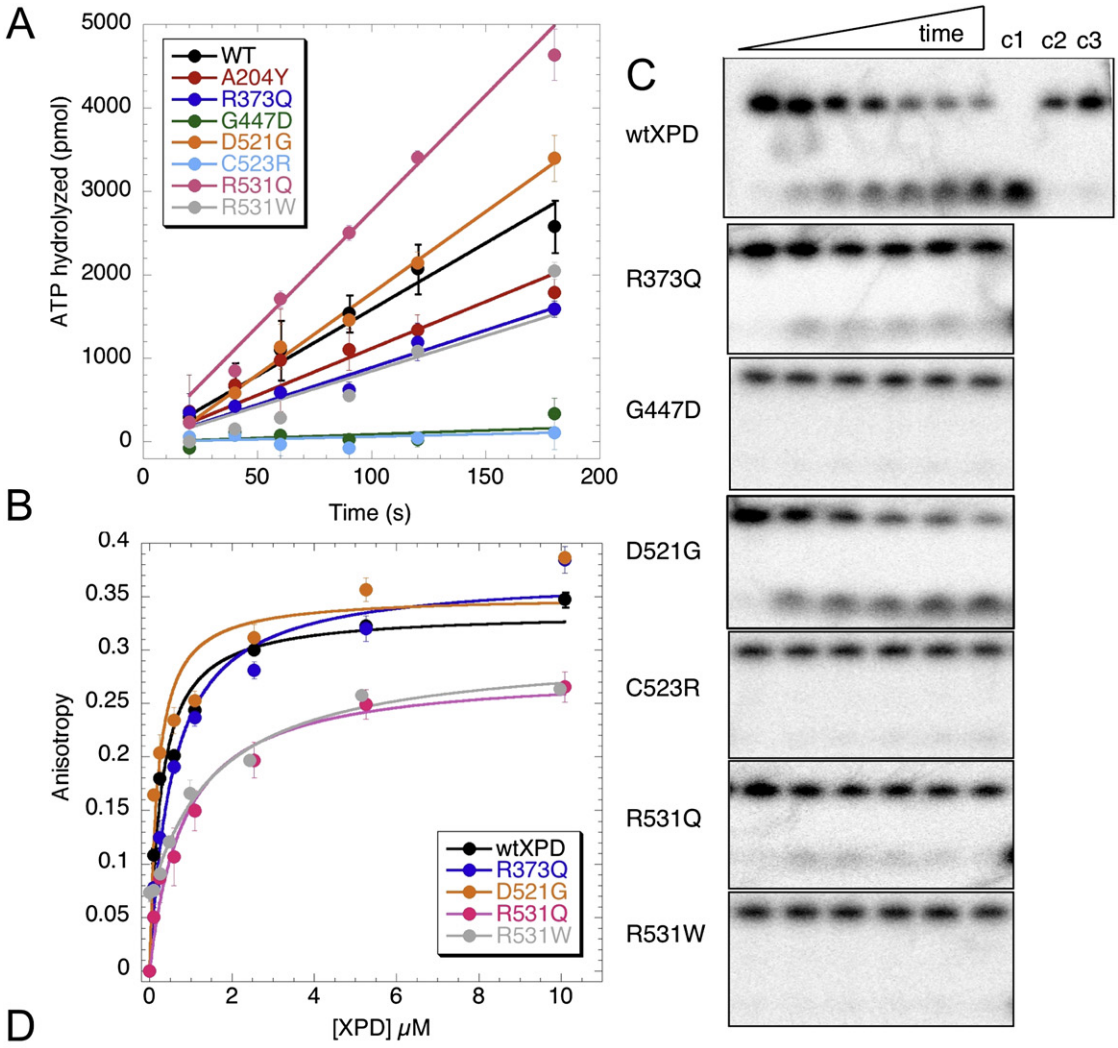

Mutation in Human	Disease	StoXPD	Mutation in *SacXPD*	ATPase activity (% wild-type)	Apparent K_D ssDNA 15T (μM)	Helicase activity
Wild-type				100 ± 7	0.27	++
C259Y	TTD	A206	A204Y	70 ± 7	nd	++
R511Q	XP	R365	R373Q	56 ± 4	0.55	-
G602D	XP/CS	A438	G447D	6 ± 2	nd	-
D673G	TTD	D511	D521G	130 ± 3	0.19	++
G675R	XP/CS	V513	C523R	4 ± 2	nd	-
R683Q	XP	R521	R531Q	170 ± 5	0.82	-
R683W	XP	R521	R531W	53 ± 2	1.6	-

Figure 4. Biochemical Characterization of Selected Mutations of XPD

(A) Plot of the ssDNA-stimulated ATPase activities of the indicated wild-type and mutant proteins of *S. acidocaldarius* XPD. Relative ATPase activities are shown in 4D. Experiments were carried out in triplicate and means with standard errors are shown. Data were fitted by a linear fit. Rates expressed as a percentage of the wild-type rate with standard errors are shown in (D).

in markedly lowered levels of TFIIH in cells, whereas XP linked mutants generally do not (Botta et al., 2002; Dubaele et al., 2003). However, eukaryotic XPD is only fully active when assembled in the TFIIH complex, and is specifically stimulated by its interaction with p44. It has therefore not been possible to disentangle the mutations that target the helicase activity directly from those which destabilize protein:protein interactions important for activity. Thus, both XP and TTD linked mutations reduce XPD helicase activity and consequently NER capacity (Nishiwaki et al., 2004). However, XP patients are highly cancer-prone while TTD patients are not. This discrepancy has been explained as a consequence of the subtle interplay between NER and transcriptional defects in TTD patients, with the suggestion that the rapid cell death and early senescence caused by TTD is protective against cancer (Andressoo et al., 2006).

Since the archaeal XPD is fully functional in the absence of protein partners, it is a useful model system in which to deconvolute the role of mutations. A priori, one can make three predictions: first, that mutations that affect protein:protein interactions would in general target less highly conserved residues in the archaeal enzyme and result in negligible phenotypes. Second, mutations that destabilize the XPD protein structure directly, rather than disrupt complex formation, are unlikely to be conserved but should give a detectable phenotype. Finally, mutations that inactivate the helicase activity while preserving the stability of TFIIH should target conserved residues in the archaeal enzyme and reduce the archaeal helicase activity. As described above, bioinformatic comparisons and biochemical assays of mutant proteins confirm all three of these predictions.

Our data are in broad agreement with the work of Egly and coworkers (Dubaele et al., 2003), who showed that TTD but not XP mutations inhibit transcription in vitro by destabilization of the TFIIH complex. These studies demonstrated that the S541R and R601W mutations do not compromise binding to p44 in vitro, consistent with our data. However, they did demonstrate a weakening of the XPD-p44 interaction for the R683W mutant. Given the clustering of these 3 residues, their distance from other residues known to interact with p44 and the XP phenotype of the R683W mutation, which has no transcriptional defect associated with it (Dubaele et al., 2003), we assume that the primary role of R683 is catalytic, and that TFIIH stability in vivo is close to normal for this mutant. Potentially, the introduction of a bulky tryptophan residue at this position has a subtle effect on human XPD stability.

In humans, XP/CS mutations combine the segmental progeria of CS with the elevated cancer risk of XP (Lehmann, 2001). The two XP/CS mutations generated in archaeal XPD both reduce the ssDNA-stimulated ATPase and therefore helicase activity significantly without reducing the protein stability. In this respect they resemble XP rather than CS mutations. This reinforces studies of reconstituted human TFIIH containing XPD with the G602D and G675R XP/CS mutations, which were both NER-deficient and active in basal transcription, in contrast to CS and TTD mutations (Dubaele et al., 2003). The challenge remains to determine why these mutations cause CS as well as XP symptoms, and how this relates to the as yet unexplained elevation in strand breakage events observed in human XP/CS cells and the XP/CS model mouse (Andressoo et al., 2006; Berneburg et al., 2000).

Mutations targetting human XPD thus give rise to a broad spectrum of pathologies, but also to a range of severity of clinical symptoms. For example, it is notable that the clinical severity of the R683W mutation is classed as severe, while that of the R683Q mutation is moderate (Botta et al., 2002). This correlates with our observation that the former mutation has a more deleterious effect on ssDNA binding affinity than the latter (Figure 4D). Levels of TFIIH are reduced in some XP patients by up to 50% without any obvious transcriptional defect, suggesting that XP mutations may also partially destabilize XPD or its protein interactions. Some TTD mutations, such as R112H, give rise to more moderate clinical symptoms than others, suggesting that differences in the degree of destabilization of XPD and/or TFIIH give rise to different phenotypes, as might be expected. A number of TTD and XP patients are compound heterozygotes with a combination of different mutations in the two copies of the XPD gene (Botta et al., 1998), complicating functional analysis. A patient with two mutant XPD alleles, leading to the mutations R112H and L485P at the amino acid level, showed symptoms of both TTD and XP (Broughton et al., 2001). Furthermore, patients with identical mutations in XPD can have quite different clinical symptoms, emphasizing the complexity of the disorders that can arise in humans (Fujimoto et al., 2005).

In conclusion, we have described the crystal structure of the DNA repair XPD helicase, the first structure of an SF2 helicase with 5′ to 3′ polarity. The structure suggests strongly that helicase polarity is determined by the direction of translocation rather than the nucleic acid binding orientation. The FeS cluster present in this helicase family can now be ascribed a structural role, stabilizing a small duplex-breaking "plowshare" domain. Finally, the structure allows the many naturally-occurring human mutations of XPD, and the three overlapping diseases that can result, to begin to be understood at a molecular level.

EXPERIMENTAL PROCEDURES

Expression and Purification of XPD from Sulfolobus Tokodaii

For crystallization trials, the *xpd* gene from *Sulfolobus tokodaii str. 7* (Kawarabayasi et al., 2001) (ST1307, uniprot entry Q971R4) was cloned into the

(B) Plot of the anisotropy changes resulting from binding of the indicated wild-type and mutant XPD proteins from *S. acidocaldarius* to a 15 nucleotide oligonucleotide tagged with a 5′ fluorescein reporter molecule. Apparent dissociation constants are shown in 4D. Experiments were carried out in triplicate and means with standard errors are shown. Data were fitted as described in the Experimental Procedures.

(C) Helicase activities of wild-type and mutant proteins of *S. acidocaldarius* XPD showing the time course of unwinding of a partial DNA duplex with a 25 nt 5′ overhang. Parental and product species were quantified by phosphoimaging and helicase activity is summarized in 4D. Control lanes are: c1, boiled DNA; c2, no ATP control; c3, no XPD control.

(D) Summary of the biochemical properties of the wild-type and mutant proteins of *S. acidocaldarius* XPD. Equivalent numbering for the human and *S. tokodaii* XPD homologs are also indicated. Helicase activity is scored as "++" for near-wild-type levels and "−" for completely inactive mutants. The A204Y mutant was active but temperature-sensitive, as described in Figure 3E. nd, not determined.

pDEST14 vector using a modified Gateway cloning system (Seetharamappa et al., 2007). The cloned gene contained a TEV protease cleavable N-terminal 6x histidine tag. After removal of the tag, the purified XPD had one extra glycine at the N-terminus. The XPD protein was expressed in *E. coli* strain C43 (DE3). The transformed *E. coli* cells were grown in one liter of LB medium containing 100 μg/ ml of ampicillin to an OD_{600} = 0.6 and induced with 0.4 mM IPTG overnight at 25°C. Histidine-tagged XPD was purified using the automated workflow of the Scottish Structural Proteomics Facility. This utilized two steps of nickel affinity chromatography intervened by a TEV cleavage step to remove the tag and followed by gel filtration chromatography in buffer containing 10 mM Tris (pH 7.5) and 150 mM NaCl, as described previously (Seetharamappa et al., 2007). The purified recombinant XPD protein was concentrated to 10 mg ml^{-1} and the protein identity was confirmed by mass spectrometry. The selenomethionine variant of XPD was expressed using the methionine biosynthesis inhibition method (Guerrero et al., 2001) and purified as described for the wild-type with the only exception that purification buffers contained 5 mM 2-mercaptomethanol.

Protein Purification, Site-Directed Mutagenesis, ATPase, and Helicase Assays

For biochemical analyses of wild-type and mutant XPD variants, the XPD protein from *S. acidocaldarius* was utilized. The protein was expressed and purified as described previously (Rudolf et al., 2006). Site-directed mutant forms of the protein were constructed using the Quikchange protocol (Stratagene), sequenced fully to ensure sequence integrity and purified as for the wild-type enzyme. The oligonucleotide sequences used to construct the mutants are available from the corresponding author on request. ATPase and helicase assays were carried out as described previously (Rudolf et al., 2006).

Structural Biology

Initial crystallization conditions were obtained with sitting-drop vapor diffusion using several 96-condition crystal screening kits at 20°C with a protein concentration of 10 mg ml^{-1}. Crystals appeared within 4 days in condition 30 of the JMAC screen, a PEG-based screen developed in house (S.A.M., unpublished data) (15% PEG 8K, 0.2 M Na-K-Phosphate, 0.1 M Na-Acetate, [pH 5.6]). Optimization of this condition yielded single crystals from hanging drop experiments using a mixture of 1 μl of the protein (4 mg ml^{-1}) and 0.5 μl of precipitant solution containing 15% PEG 8K, 0.15 M Na-K-Phosphate, 0.1 M Na-Acetate, (pH 5.6). The crystal used for refinement of the native structure was soaked in a cryoprotecting solution containing 20% PEG 8K, 0.1 M Na-K-Phosphate, 0.1 M Na-Acetate, (pH 5.6), 20% PEG 400, mounted in a loop and then immediately cooled to 100 K. Diffraction data were collected at Diamond beamline I03 in two passes. A high resolution pass to a resolution of 2.25Å was collected as a total of 200 images with 10 s exposures for 0.5° oscillations. A low resolution pass to a resolution of 3.3 Å was collected as 180 images with 2.5 s exposure for 1.0° oscillations. The data were indexed, integrated and scaled using HKL2000 (Otwinowski and Minor, 1997). A data set to 2.25 Å was recorded with the space group determined as $P2_12_12$. To determine the phases, Se-Met crystals were obtained with the precipitant 18% PEG 8K, 0.2 M Na-K-Phosphate, 0.1 M Na-Acetate, (pH 5.6) using microseeding. The SeMet crystal was prepared in the same manner as the native crystal for data collection. A two wavelength MAD data set (peak and high energy remote) was collected at ESRF beamline BM14 to a resolution of 2.7 Å. The two SeMet data sets were indexed, integrated and scaled using XDS and XSCALE (Kabsch, 1993). 11 out of 13 possible selenium sites were located by SHELXC and SHELXD (Schneider and Sheldrick, 2002) giving initial phases with a figure of merit of 0.275 to 3.2 Å The initial phases were extended to 2.7 Å with a figure of merit of 0.53 by SHELXE (Schneider and Sheldrick, 2002). The phases were transferred to the native data and extended to 2.25 Å using DM (Cowtan, 1994). A model with 278 residues was built by hand, input to ARP/warp (Perrakis et al., 1999) and finished manually. The structure was refined using REFMAC5 and manually rebuilt with XFIT (McRee, 1999) and COOT (Emsley and Cowtan, 2004). Simulated annealings were performed using CNS (Brunger et al., 1998) and analyzed by superposition using Sequoia (Bruns et al., 1999). Validation was performed using the Molprobity server (Davis et al., 2007).

DNA Binding Assays

The DNA binding affinity of XPD was determined at 20°C using a Cary Eclipse fluorimeter (Varian) with automatic polarizer (excitation, 490 nm; emission, 535 nm). The excitation pathlength was 10 nm, the emission pathlength 2 nm and excitation slitwidth 5 nm. For direct titration, 20 nM 5′-fluorescein labeled 15-mer oligonucleotide (5′-TCGGAGTACAGTGGG) was equilibrated in 150 μl anisotropy buffer (20 mM HEPES [pH 7.1], 100 mM NaCl, 1 mM DTT, 0.01% Triton X-100). Anisotropy and total fluorescence intensity were measured in parallel following each protein addition and the effects of dilution were corrected. To minimise rotational effects on fluorescence intensity, "magic angle" conditions were used. Each protein titration was repeated in triplicate. Data were fitted to the equation below using KaleidaGraph (Synergy Software):

$$A = A_{min} + \left((D + E + K_D) - \left((D + E + K_D)^2 - (4DE)\right)^{1/2}\right)(A_{max} - A_{min})/(2D)$$

where A, anisotropy; E, total protein concentration; D, total DNA concentration; A_{min} (minimum anisotropy), anisotropy of free DNA; A_{max} (maximum anisotropy), anisotropy of the DNA-protein complex; K_D, the dissociation constant. A 1:1 interaction between protein and DNA was assumed.

ACCESSION NUMBERS

The PDB code for the XPD coordinates is 2VL7.

SUPPLEMENTAL DATA

Supplemental Data include four figures and can be found with this article online at http://www.cell.com/cgi/content/full/133/5/801/DC1/.

ACKNOWLEDGMENTS

The structure of XPD was solved by the Scottish Structural Proteomics Facility, which is funded by the Scottish Funding Council and Biotechnology and Biological Sciences Research Council. The biochemical studies of XPD were supported by Cancer Research UK. We thank Michal Zawadzki for technical help and Catherine Botting for mass spectrometry services, which are funded at St. Andrews by the Wellcome Trust. Thanks to John Tainer for communicating data prior to publication.

Received: February 13, 2008
Revised: April 7, 2008
Accepted: April 22, 2008
Published: May 29, 2008

REFERENCES

Andressoo, J.O., Mitchell, J.R., de Wit, J., Hoogstraten, D., Volker, M., Toussaint, W., Speksnijder, E., Beems, R.B., van Steeg, H., Jans, J., et al. (2006). An Xpd mouse model for the combined xeroderma pigmentosum/Cockayne syndrome exhibiting both cancer predisposition and segmental progeria. Cancer Cell *10*, 121–132.

Berneburg, M., Clingen, P.H., Harcourt, S.A., Lowe, J.E., Taylor, E.M., Green, M.H., Krutmann, J., Arlett, C.F., and Lehmann, A.R. (2000). The cancer-free phenotype in trichothiodystrophy is unrelated to its repair defect. Cancer Res. *60*, 431–438.

Boal, A.K., Yavin, E., Lukianova, O.A., O'Shea, V.L., David, S.S., and Barton, J.K. (2005). DNA-bound redox activity of DNA repair glycosylases containing [4Fe-4S] clusters. Biochemistry *44*, 8397–8407.

Botta, E., Nardo, T., Broughton, B.C., Marinoni, S., Lehmann, A.R., and Stefanini, M. (1998). Analysis of mutations in the XPD gene in Italian patients with trichothiodystrophy: site of mutation correlates with repair deficiency, but gene dosage appears to determine clinical severity. Am. J. Hum. Genet. *63*, 1036–1048.

Botta, E., Nardo, T., Lehmann, A.R., Egly, J.M., Pedrini, A.M., and Stefanini, M. (2002). Reduced level of the repair/transcription factor TFIIH in trichothiodystrophy. Hum. Mol. Genet. *11*, 2919–2928.

Broughton, B.C., Berneburg, M., Fawcett, H., Taylor, E.M., Arlett, C.F., Nardo, T., Stefanini, M., Menefee, E., Price, V.H., Queille, S., et al. (2001). Two individuals with features of both xeroderma pigmentosum and trichothiodystrophy highlight the complexity of the clinical outcomes of mutations in the XPD gene. Hum. Mol. Genet. *10*, 2539–2547.

Brunger, A.T., Adams, P.D., Clore, G.M., DeLano, W.L., Gros, P., Grosse-Kunstleve, R.W., Jiang, J.S., Kuszewski, J., Nilges, M., Pannu, N.S., et al. (1998). Crystallography & NMR system: A new software suite for macromolecular structure determination. Acta Crystallogr. D Biol. Crystallogr. *54*, 905–921.

Bruns, C.M., Hubatsch, I., Ridderstrom, M., Mannervik, B., and Tainer, J.A. (1999). Human glutathione transferase A4–4 crystal structures and mutagenesis reveal the basis of high catalytic efficiency with toxic lipid peroxidation products. J. Mol. Biol. *288*, 427–439.

Buttner, K., Nehring, S., and Hopfner, K.P. (2007). Structural basis for DNA duplex separation by a superfamily-2 helicase. Nat. Struct. Mol. Biol. *14*, 647–652.

Chen, J., Larochelle, S., Li, X., and Suter, B. (2003). Xpd/Ercc2 regulates CAK activity and mitotic progression. Nature *424*, 228–232.

Chen, J., and Suter, B. (2003). Xpd, a structural bridge and a functional link. Cell Cycle *2*, 503–506.

Cowtan, K. (1994). An automated procedure for phase improvement by density modification. Joint CCP4 and ESF-EACBM Newsletter on Protein Crystallography *31*, 34–38.

Davis, I.W., Leaver-Fay, A., Chen, V.B., Block, J.N., Kapral, G.J., Wang, X., Murray, L.W., Arendall, W.B., 3rd, Snoeyink, J., Richardson, J.S., et al. (2007). MolProbity: all-atom contacts and structure validation for proteins and nucleic acids. Nucleic Acids Res. *35*, W375–W383.

de Boer, J., Andressoo, J.O., de Wit, J., Huijmans, J., Beems, R.B., van Steeg, H., Weeda, G., van der Horst, G.T., van Leeuwen, W., Themmen, A.P., et al. (2002). Premature aging in mice deficient in DNA repair and transcription. Science *296*, 1276–1279.

Dubaele, S., Proietti De Santis, L., Bienstock, R.J., Keriel, A., Stefanini, M., Van Houten, B., and Egly, J.M. (2003). Basal transcription defect discriminates between xeroderma pigmentosum and trichothiodystrophy in XPD patients. Mol. Cell *11*, 1635–1646.

Dupuy, J.M., and Lafforet, D. (1978). Xeroderma pigmentosum and Cockayne syndrome. Pediatrics *61*, 675–676.

Emsley, P., and Cowtan, K. (2004). Coot: model-building tools for molecular graphics. Acta Crystallogr. D Biol. Crystallogr. *60*, 2126–2132.

Fujimoto, M., Leech, S.N., Theron, T., Mori, M., Fawcett, H., Botta, E., Nozaki, Y., Yamagata, T., Moriwaki, S., Stefanini, M., et al. (2005). Two new XPD patients compound heterozygous for the same mutation demonstrate diverse clinical features. J. Invest. Dermatol. *125*, 86–92.

Gorbalenya, A.E., and Koonin, E.V. (1993). Helicases: amino acid sequence comparisons and structure-function relationships. Curr. Opin. Struct. Biol. *3*, 419–429.

Guerrero, S.A., Hecht, H.J., Hofmann, B., Biebl, H., and Singh, M. (2001). Production of selenomethionine-labelled proteins using simplified culture conditions and generally applicable host/vector systems. Appl. Microbiol. Biotechnol. *56*, 718–723.

Hinks, J.A., Evans, M.C., De Miguel, Y., Sartori, A.A., Jiricny, J., and Pearl, L.H. (2002). An iron-sulfur cluster in the family 4 uracil-DNA glycosylases. J. Biol. Chem. *277*, 16936–16940.

Hirata, A., Klein, B.J., and Murakami, K.S. (2008). The X-ray crystal structure of RNA polymerase from Archaea. Nature *451*, 851–854.

Kabsch, W. (1993). Automatic processing of rotation diffraction data from crystals of initially unknown symmetry and cell constants. J. Appl. Cryst. *26*, 795–800.

Kawarabayasi, Y., Hino, Y., Horikawa, H., Jin-no, K., Takahashi, M., Sekine, M., Baba, S., Ankai, A., Kosugi, H., Hosoyama, A., et al. (2001). Complete genome sequence of an aerobic thermoacidophilic crenarchaeon, Sulfolobus tokodaii strain7. DNA Res. *8*, 123–140.

Kelman, Z., and White, M.F. (2005). Archaeal DNA replication and repair. Curr. Opin. Microbiol. *8*, 669–676.

Kim, J.L., Morgenstern, K.A., Griffith, J.P., Dwyer, M.D., Thomson, J.A., Murcko, M.A., Lin, C., and Caron, P.R. (1998). Hepatitis C virus NS3 RNA helicase domain with a bound oligonucleotide: the crystal structure provides insights into the mode of unwinding. Structure *6*, 89–100.

Klinge, S., Hirst, J., Maman, J.D., Krude, T., and Pellegrini, L. (2007). An iron-sulfur domain of the eukaryotic primase is essential for RNA primer synthesis. Nat. Struct. Mol. Biol. *14*, 875–877.

Kuo, C.F., McRee, D.E., Fisher, C.L., O'Handley, S.F., Cunningham, R.P., and Tainer, J.A. (1992). Atomic structure of the DNA repair [4Fe-4S] enzyme endonuclease III. Science *258*, 434–440.

Lee, B.S., Bi, L., Garfinkel, D.J., and Bailis, A.M. (2000). Nucleotide excision repair/TFIIH helicases RAD3 and SSL2 inhibit short-sequence recombination and Ty1 retrotransposition by similar mechanisms. Mol. Cell. Biol. *20*, 2436–2445.

Lehmann, A.R. (2001). The xeroderma pigmentosum group D (XPD) gene: one gene, two functions, three diseases. Genes Dev. *15*, 15–23.

Lehmann, A.R. (2003). DNA repair-deficient diseases, xeroderma pigmentosum, Cockayne syndrome and trichothiodystrophy. Biochimie *85*, 1101–1111.

McRee, D.E. (1999). XtalView/Xfit–A versatile program for manipulating atomic coordinates and electron density. J. Struct. Biol. *125*, 156–165.

Nishiwaki, Y., Kobayashi, N., Imoto, K., Iwamoto, T.A., Yamamoto, A., Katsumi, S., Shirai, T., Sugiura, S., Nakamura, Y., Sarasin, A., et al. (2004). Trichothiodystrophy fibroblasts are deficient in the repair of ultraviolet-induced cyclobutane pyrimidine dimers and (6–4)photoproducts. J. Invest. Dermatol. *122*, 526–532.

Otwinowski, Z., and Minor, W. (1997). Processing of X-ray diffraction data collected in oscillation mode. In Macromolecular Crystallography, part A, C.W.J. Carter and R.M. Sweet, eds. (New York: Academic Press), pp. 307–326.

Perrakis, A., Morris, R., and Lamzin, V.S. (1999). Automated protein model building combined with iterative structure refinement. Nat. Struct. Biol. *6*, 458–463.

Pugh, R.A., Honda, M., Leesley, H., Thomas, A., Lin, Y., Nilges, M.J., Cann, I.K., and Spies, M. (2008). The Iron-containing Domain Is Essential in Rad3 Helicases for Coupling of ATP Hydrolysis to DNA Translocation and for Targeting the Helicase to the Single-stranded DNA-Double-stranded DNA Junction. J. Biol. Chem. *283*, 1732–1743.

Rudolf, J., Makrantoni, V., Ingledew, W.J., Stark, M.J., and White, M.F. (2006). The DNA repair helicases XPD and FancJ have essential iron-sulfur domains. Mol. Cell *23*, 801–808.

Schneider, T.R., and Sheldrick, G.M. (2002). Substructure solution with SHELXD. Acta Crystallogr. D Biol. Crystallogr. *58*, 1772–1779.

Seetharamappa, J., Oke, M., Liu, H., McMahon, S.A., Johnson, K.A., Carter, L., Dorward, M., Zawadzki, M., Overton, I.M., van Niekirk, C.A., et al. (2007). Purification, crystallization and data collection of methicillin-resistant Staphylococcus aureus Sar2676, a pantothenate synthetase. Acta Crystallogr Sect F Struct Biol Cryst Commun *63*, 488–491.

Singleton, M.R., Dillingham, M.S., Gaudier, M., Kowalczykowski, S.C., and Wigley, D.B. (2004). Crystal structure of RecBCD enzyme reveals a machine for processing DNA breaks. Nature *432*, 187–193.

Singleton, M.R., Dillingham, M.S., and Wigley, D.B. (2007). Structure and Mechanism of Helicases and Nucleic Acid Translocases. Annu. Rev. Biochem. *76*, 23–50.

Singleton, M.R., and Wigley, D.B. (2002). Modularity and specialization in superfamily 1 and 2 helicases. J. Bacteriol. *184*, 1819–1826.

Soultanas, P., Dillingham, M.S., Wiley, P., Webb, M.R., and Wigley, D.B. (2000). Uncoupling DNA translocation and helicase activity in PcrA: direct evidence for an active mechanism. EMBO J. *19*, 3799–3810.

Taylor, E.M., Broughton, B.C., Botta, E., Stefanini, M., Sarasin, A., Jaspers, N.G., Fawcett, H., Harcourt, S.A., Arlett, C.F., and Lehmann, A.R. (1997). Xeroderma pigmentosum and trichothiodystrophy are associated with different mutations in the XPD (ERCC2) repair/transcription gene. Proc. Natl. Acad. Sci. USA *94*, 8658–8663.

Theis, K., Chen, P.J., Skorvaga, M., Van Houten, B., and Kisker, C. (1999). Crystal structure of UvrB, a DNA helicase adapted for nucleotide excision repair. EMBO J. *18*, 6899–6907.

Theron, T., Fousteri, M.I., Volker, M., Harries, L.W., Botta, E., Stefanini, M., Fujimoto, M., Andressoo, J.O., Mitchell, J., Jaspers, N.G., et al. (2005). Transcription-associated breaks in xeroderma pigmentosum group D cells from patients with combined features of xeroderma pigmentosum and Cockayne syndrome. Mol. Cell. Biol. *25*, 8368–8378.

van Hoffen, A., Kalle, W.H., de Jong-Versteeg, A., Lehmann, A.R., van Zeeland, A.A., and Mullenders, L.H. (1999). Cells from XP-D and XP-D-CS patients exhibit equally inefficient repair of UV-induced damage in transcribed genes but different capacity to recover UV-inhibited transcription. Nucleic Acids Res. *27*, 2898–2904.

Vermeulen, W., Rademakers, S., Jaspers, N.G., Appeldoorn, E., Raams, A., Klein, B., Kleijer, W.J., Hansen, L.K., and Hoeijmakers, J.H. (2001). A temperature-sensitive disorder in basal transcription and DNA repair in humans. Nat. Genet. *27*, 299–303.

Voloshin, O.N., and Camerini-Otero, R.D. (2007). The DinG protein from Escherichia coli is a structure-specific helicase. J. Biol. Chem. *282*, 18437–18447.

Winkler, G.S., Araujo, S.J., Fiedler, U., Vermeulen, W., Coin, F., Egly, J.M., Hoeijmakers, J.H., Wood, R.D., Timmers, H.T., and Weeda, G. (2000). TFIIH with inactive XPD helicase functions in transcription initiation but is defective in DNA repair. J. Biol. Chem. *275*, 4258–4266.